Laboratory study of nitrate photolysis in Antarctic snow. I. Observed quantum yield, domain of photolysis, and secondary chemistry

Carl Meusinger, Tesfaye Berhanu, Joseph Erbland, Joel Savarino, Matthew Johnson

RESEARCH ARTICLE | JUNE 24 2014

Laboratory study of nitrate photolysis in Antarctic snow. I. Observed quantum yield, domain of photolysis, and secondary chemistry

Carl Meusinger ; Tesfaye A. Berhanu; Joseph Erbland; Joel Savarino; Matthew S. Johnson

J. Chem. Phys. 140, 244305 (2014)
https://doi.org/10.1063/1.4882898

Laboratory study of nitrate photolysis in Antarctic snow. I. Observed quantum yield, domain of photolysis, and secondary chemistry

Carl Meusinger,[1] Tesfaye A. Berhanu,[2,3] Joseph Erbland,[2,3] Joel Savarino,[2,3,a)] and Matthew S. Johnson[1]
[1]*Department of Chemistry, University of Copenhagen, Copenhagen, Denmark*
[2]*Univ. Grenoble Alpes, LGGE, F-38000 Grenoble, France*
[3]*CNRS, LGGE, F-38000 Grenoble, France*

(Received 18 December 2013; accepted 29 May 2014; published online 24 June 2014)

Post-depositional processes alter nitrate concentration and nitrate isotopic composition in the top layers of snow at sites with low snow accumulation rates, such as Dome C, Antarctica. Available nitrate ice core records can provide input for studying past atmospheres and climate if such processes are understood. It has been shown that photolysis of nitrate in the snowpack plays a major role in nitrate loss and that the photolysis products have a significant influence on the local troposphere as well as on other species in the snow. Reported quantum yields for the main reaction spans orders of magnitude – apparently a result of whether nitrate is located at the air-ice interface or in the ice matrix – constituting the largest uncertainty in models of snowpack NO_x emissions. Here, a laboratory study is presented that uses snow from Dome C and minimizes effects of desorption and recombination by flushing the snow during irradiation with UV light. A selection of UV filters allowed examination of the effects of the 200 and 305 nm absorption bands of nitrate. Nitrate concentration and photon flux were measured in the snow. The quantum yield for loss of nitrate was observed to decrease from 0.44 to 0.003 within what corresponds to days of UV exposure in Antarctica. The superposition of photolysis in two photochemical domains of nitrate in snow is proposed: one of photolabile nitrate, and one of buried nitrate. The difference lies in the ability of reaction products to escape the snow crystal, versus undergoing secondary (recombination) chemistry. Modeled NO_x emissions may increase significantly above measured values due to the observed quantum yield in this study. The apparent quantum yield in the 200 nm band was found to be ∼1%, much lower than reported for aqueous chemistry. A companion paper presents an analysis of the change in isotopic composition of snowpack nitrate based on the same samples as in this study. [http://dx.doi.org/10.1063/1.4882898]

I. INTRODUCTION

The nitrogen cycle is central to atmospheric chemistry as it governs photochemistry and oxidant budgets.[1,2] The photochemistry of nitrogen oxides ($NO_x = NO + NO_2$) produces ozone in the troposphere and the NO_x reactions are the most important catalytic cycle removing ozone from the stratosphere.[3] Oxygen atoms are exchanged rapidly between ozone and NO_x, with the result that polar NO_x contains material from atmospheric ozone. Therefore, information on the atmosphere's oxidative capacity is stored in the main sink of the cycle, deposited nitrate.[4] The information contained in ice core records of nitrate buried in polar regions may help in reconstructing the oxidative conditions prevailing in past climatic conditions[5] and in better constraining the nitrogen budget.[6,7] Nitrate is detected easily using, e.g., ion chromatography, but post-depositional processes in the snow alter the nitrate concentration and prevent interpretation of the record at sites with low snow accumulation rates.[8–10] Nitrate profiles in the top centimeters of snow from, e.g., Dome C, Antarctica, show a significant decrease with depth,[11] while field measurements in summer show increased NO_x emissions above the snow pack at the same locations.[12,13] Elevated polar NO_x levels are suggested to play a central role in remote boundary layer chemistry where they can lead to net production of ozone.[14] Laboratory experiments and field studies indicate that desorption and photolysis of nitrate in snow play a key role.

The following reaction known from the aqueous phase is generally assumed to be the dominant mechanism for nitrate photolysis in snow:

$$NO_3^- + h\nu \xrightarrow{H^+} NO_2 + OH. \quad (R1)$$

The quantum yield of associated product species formed in ice at −20 °C ranges from 0.0028 (Chu and Anastasio[15]) to 0.6 (Zhu *et al.*[16]), depending on the experimental method. Chu and Anastasio[15] froze a prepared aqueous $NaNO_3$ solution, irradiated it with UV light at wavelengths longer than 300 nm and detected the resulting OH radicals in order to report Φ_{OH}.[15] They argue that photolysis takes place in the *disordered interface* (DI, sometimes called the *quasi liquid layer*[17]). The small value they obtained for the quantum yield supports the theory that product species are preferentially

a)Electronic mail: jsavarino@lgge.obs.ujf-grenoble.fr

trapped by the aqueous cage effect (see below) potentially lowering the observed quantum yield.[18]

Zhu *et al.*[16] conducted experiments using HNO_3 adsorbed on an ice film.[16] They detected NO_2 using cavity ring-down spectroscopy and showed that both the absorption cross section of adsorbed nitrate and the quantum yield, Φ_{NO_2}, have much larger values than reported in liquid phase;[15] at 308 nm and $-20\,^{\circ}C$ the absorption cross section increases by a factor of $\sim$50 and Φ_{NO_2} increases by a factor >100. Products from adsorbed species seem to leave the ice more easily, increasing the observed quantum yield. In another experiment by the same authors, HNO_3 adsorbed on aluminum shows even higher values of Φ_{NO_2}. The authors therefore argue that the quantum yield for photolysis of HNO_3 adsorbed on ice may be even larger than 0.6 because some of the NO_2 product is dissolved in water/ice.

The difference in the reported quantum yields has a direct impact on modeling studies which try to match the measured NO_x flux from the snow pack with the underlying photochemistry. In a recent study, Frey *et al.*[13] modeled daytime NO_x emissions in the austral summer at Dome C and matched daytime observations, but under-predicted nighttime NO_x emissions by a factor of $\sim 3-4$. Such studies of the NO_x flux from the snowpack often consider only aqueous chemistry and use the smaller of the reported values for the quantum yield.[13,19,20] The good match with day-time NO_x emissions may suggest that nitrate photolysis occurs in the DI, however these studies all serve to emphasize that knowledge of the quantum yield of nitrate photolysis in snow is among the main uncertainties to current models.

A. Domain of snow photochemistry

The physical and chemical properties of species in snow are altered by their microphysical location due to differences in phase and the dielectric constant and electrical fields arising from, e.g., salt, dust, and phase boundaries, with important implications to snow-atmosphere interactions.[21,22] Potential photochemical reaction sites for chromophores in snow such as nitrate include: bulk ice, water in or on the snow, the DI, the grain boundary (where the Kelvin effect minimizes freezing), the ice surface and inside mineral dust, or sea-salt impurities. The term *domain of snow photochemistry* is used here, following Davis *et al.*,[18] to describe the microphysical properties of the region around the nitrate chromophore that affect its photodissociation. For example, the phase and ionic strength of the nearby region will modify the absorption cross section and photoproduct-cage interactions. As summarized in a recent review by Bartels-Bausch *et al.*[17] the rate constants for a given chemical reaction can differ by orders of magnitude depending on the domain of snow photochemistry.

One example of a domain-specific influence on a photochemical reaction is the *cage effect*. Following photoexcitation in liquids and ice, the surrounding medium may inhibit the initially formed primary products from escaping the cage of water molecules surrounding them. The products lose their excess energy via collisions to the water molecules and often reform the initial compound. The cage effect has been observed for many systems including organics in ice[23–25] and nitrate photolysis in aqueous solution.[26] Kurková *et al.*[24] show that the strength of the cage effect for organic compounds is a function of temperature (stronger recombination at lower temperatures) and microphysical state (frozen solutions show a cage effect at much lower temperature than artificial snow).

In the case of nitrate, there is evidence of recombination of photoproducts and of the presence of two reservoirs of nitrate which behave differently upon photoexcitation: In an early study, Dubowski *et al.*[27] report changes in the nitrate photolysis product distribution over time. The changes were associated with the depth of different layers, allowing for stronger secondary chemistry deeper in the snow. In a similar study, Beine and Anastasio[28] report changes in the photolysis rate of HOOH over time. More recently, Baergen and Donaldson[29] saw four orders of magnitude faster nitrate photolysis in grime than in aqueous solution. In addition, they observed a background signal associated with photolysis of more strongly bound nitrate. Similarly, Blunier *et al.*[30] observed a nitrate fraction which could not be photolysed, no matter the length of photolysis. Finally, Thomas *et al.*[20] set up a chemical model which reproduced NO ratios in the boundary layer (at Summit, Greenland) by assuming a fixed ratio between nitrate in the DI and in the snow grain. Davis *et al.*[18] were among the first to suggest multiple nitrate reservoirs that result in a superposition of photochemistry from different snow-photochemical domains. The microphysical location appears to control how labile nitrate is with respect to UV light in snow. Therefore, the present study distinguishes two domains of nitrate photochemistry in snow: *photolabile* nitrate and *buried* nitrate.

B. Reaction mechanism

Several nitrate photolysis reaction mechanisms have been proposed.[31–35] An overview of the main reactions of concern to this work is shown in Figure 1. The complete mechanism

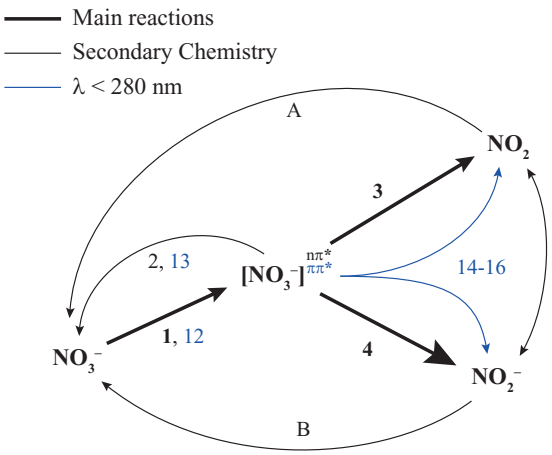

FIG. 1. Scheme of the main chemical reactions. The square brackets denote a solvent cage. Product species like NO_2 may leave the system as gases, undergo photolysis or take part in secondary reactions as indicated. Blue color indicates reactions only possible at certain photolysis wavelengths. The numbers refer to reactions in the Appendix; A and B stand for reactions (A5)–(A11) and (A17).

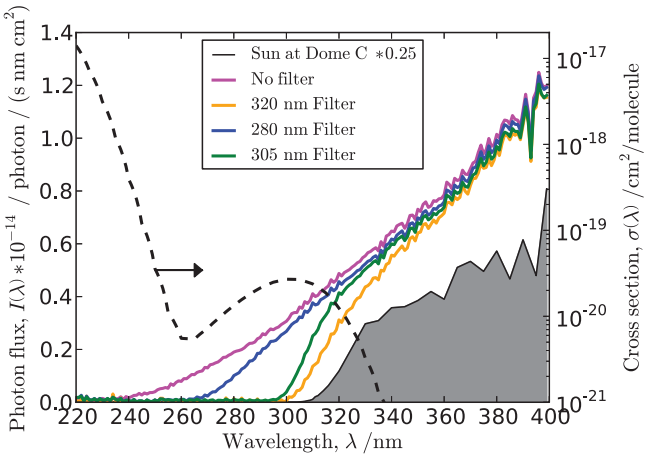

FIG. 2. Photon flux of different sources (left axis) and the liquid phase nitrate absorption cross section (dashed line, right axis). The modeled actinic flux of the sun at Dome C (noon of 1 January 2012, in Antarctica at 3000 m elevation, with an overhead ozone column of 300 Dobson Units calculated using the TUV model[36]) and the Xe lamp's spectrum measured 1 cm inside the snow (with different filters in place, cf. legend). Note the logarithmic scale on the right.

is described in the Appendix, and a short summary is given here.

The aqueous chemistry of nitrogen species is used as a starting point.[17,31] In the aqueous phase, the nitrate ion absorbs light over a wide range of wavelengths and shows two prominent absorption bands at around 200 and 305 nm, as shown in Figure 2. The 200 nm band is about 1000 times stronger than the 305 nm absorption band, but typically plays a smaller role in environmental studies due to the onset of the actinic flux at Earth's surface around 300 nm, cf. Figure 2.

Reaction (R1) corresponds to reactions (A1) and (A3) in Figure 1 and the Appendix. NO_2 can enter the gas phase and leave the system, consistent with NO_2 fluxes from the snowpack.[13,14] NO_2 can also be photolysed or undergo further reaction. Pathways A and B in Figure 1 show reformation of nitrate from its own photoproducts, cf. reactions (A5)–(A11) and (A17) in the Appendix.

Aqueous chemistry on its own may not resemble nitrate snow-phase chemistry for two reasons: (i) the superposition of photochemistry of different nitrate domains and (ii) the recombination of nitrate due to secondary chemistry (pathways A and B in Figure 1) and the solvent cage (reaction (A2)). Both recombination reactions and the cage effect may lower observed quantum yields depending on experimental conditions as the reactant might reform and show reaction rates that depend on photoproduct concentrations. Therefore, the presented mechanism does not include reformation rates. Quantum yields for specific products and for the loss of nitrate are experimentally determined quantities and therefore the effects of the nitrate domains and recombination chemistry are implicitly included, unless the experiments allow to exclude them explicitly.

Light of wavelengths around 200 nm is not present in the troposphere, but plays a role in the stratosphere at sufficient height. If the deposited nitrate in snow at Dome C originates from polar stratospheric clouds (typical altitude 15–20 km), it has been exposed to radiation of such wavelengths. At wavelengths shorter than 300 nm isomerization forming peroxynitrite is added as an additional pathway to the overall reaction scheme at longer wavelengths. Strong cage effects and a product pool that might recombine to nitrate are also present at higher excitation energies, cf. Figure 1 and the Appendix.

The goal of this work is to study nitrate photolysis in natural snow under controlled conditions including light spectrum and temperature while flushing the snow to test for desorption and recombination. This paper describes the setup, sample handling, data analysis, and interpretation in terms of photochemistry, while the companion paper discusses the results for the stable isotopic composition of nitrate for the same samples. In the present study, the quantum yield is determined by measuring the photon flux inside the snow and the nitrate concentrations before and after illumination with a Xenon lamp. Two hypotheses are tested:

- Since the rate of reformation of nitrate depends on the concentration of nitrate photoproducts, the quantum yield will be dependent on light intensity.
- Since the different domains of nitrate in snow (photolabile vs. buried) show different behavior under UV exposure, these two pools account for the large variation reported for values of the quantum yield.

II. THEORY

A. Mass-balance equation

Considering the reaction mechanism in Figure 1, the mass-balance equation for nitrate is as follows:

$$\frac{\mathrm{d}\,c\left(\mathrm{NO_3^-}\right)}{\mathrm{d}t} = -c\left(\mathrm{NO_3^-}\right) J_1 \left(\Phi_2 + \Phi_3 + \Phi_4\right) + c(\mathrm{NO_2})\, k_A + c\left(\mathrm{NO_2^-}\right) k_B + c\left(\mathrm{NO_3^-}\right) J_1 \Phi_2. \quad (1)$$

Here, c denotes concentrations; negative terms indicate nitrate loss, and positive terms nitrate production. Quantities denoted by J are *first-order rate constants* and those denoted by k are reaction rate constants. The subscripts refer to the reactions given in Figure 1 and in the Appendix. J_1 is the rate constant of photoexcitation in the $n\pi^*$ path (305 nm band) and J_{12} of the photoexcitation in the $\pi\pi^*$ path (200 nm band). The $n\pi^*$ excited NO_3^- may decay to reagents (reaction (A2)), or the nitrate may be lost by reactions (A3) and (A4). Thus, the primary quantum yield for nitrate loss is $(\Phi_3 + \Phi_4)$. The effect of reaction (A2), relaxation of $NO_3^{-n\pi^*}$ to NO_3^-, is accounted for by the last summand in Eq. (1). Subscripts A and B indicate secondary chemistry reforming nitrate which is not resolved in this study, cf. the Appendix.

In the present study, only nitrate concentrations are measured and therefore the individual terms in Eq. (1) can only be assessed indirectly. Nitrate photolysis in snow is assumed here to be a single-step, unidirectional reaction and the right-hand side of Eq. (1) can be reduced to a single loss term giving

via integration

$$J^* = \frac{-\ln f}{t}. \quad (2)$$

Equation (2) relates the apparent photolysis rate constant, J^*, to the photolysis time, t, and to the measured fraction of nitrate remaining in snow, $f = w_i\left(NO_3^-\right)/w_\circ\left(NO_3^-\right)$, with measured nitrate mass fractions, $w\left(NO_3^-\right)$ (in ppbw = ng/g). The subscript i denotes any form of extent, e.g., photolysis time, and $\circ$ denotes the initial sample.

The concept of *apparent* quantities (denoted by the * symbol) is used to distinguish the apparent photolysis rate constant (derived from measured nitrate fractions in Eq. (2)) from the primary photolysis rate constants in Eq. (1). Erbland *et al.*[37] used apparent quantities in a similar way to describe isotopic measurements in the field which incorporated several complex, simultaneous underlying processes.

B. Apparent photolysis rate constant and quantum yield

The apparent nitrate photolysis rate constant, J^* (units of s^{-1}), is defined by

$$J^*(z) = \int I(\lambda, z)\,\Phi^*(\lambda, z)\,\sigma(\lambda)\,d\lambda. \quad (3)$$

Here, I is the *photon flux* in photons/(cm^2 s nm), σ is the nitrate *absorption cross section* in cm^2/molecule, and Φ^* is the *apparent quantum yield* (in molecules/photon). The quantities in Eq. (3) are functions of depth in the snow layer, z, and wavelength, λ, to emphasize the importance of these parameters. The dependence on temperature, T, and light beam angle is neglected as experiments are done at constant temperature and always with the light beam normal to the snow surface, see below. The quantities in Eq. (3) have been subject to substantial research in the past. The photon flux, I as a function of depth, for instance, is a nonlinear function of absorption and scattering in snow[19,36,38] as discussed in more detail in Sec. II D. Also, the spectrum of a Xe lamp (used here and in most other studies) is significantly different from that of the sun resulting in different photolysis rates.[11,39] The absorption cross section and product quantum yields for nitrate in the liquid phase and of adsorbed HNO_3 have been measured. However, it is not certain to what degree those measurements are applicable to nitrate in snow, as the microphysical location of nitrate in ice seems to affect reported values.[15,16] The present study uses absorption cross sections from aqueous phase measurements for 220–340 nm at room temperature by Burley and Johnston[40] and at >340 nm for 278 K by Chu and Anastasio[15] Figure 2 shows some of the quantities of interest for nitrate photolysis.

The apparent quantum yield, Φ^*, was introduced into Eq. (3) to account for processes in addition to photolysis that alter the nitrate concentration and is therefore also called *quantum yield for loss of nitrate*. Φ^* implicitly includes the k_A and k_B terms in Eq. (1) as well as all J terms. Furthermore, differences in reaction kinetics between different domains of nitrate photolysis in snow are also included in Φ^*. In this way, $c(NO_3^-)$ and I – both of which can be determined in the field – are considered in relation to each other. In contrast to other studies on the products of photodissociation,[15,16] the present study focuses on the fate of nitrate in Antarctic snow.

Assuming that the quantum yield is independent of λ,[15] Eq. (3) can be rearranged to give

$$\Phi^*(t, z) = \frac{J^*(t, z)}{\int I(\lambda, z)\,\sigma(\lambda)\,d\lambda}. \quad (4)$$

Equation (4) allows derivation of the apparent quantum yield from the measured photon flux, I, and an apparent J^* which was calculated from the measured nitrate concentration in snow. Since I was measured inside the snow, chromophores do not affect I further. As indicated here and shown later, both J^* and Φ^* are dependent on depth in the snow and photolysis time.

C. 200 and 305 nm absorption bands

A Xe lamp was used in the present work, allowing study of both the 200 and 305 nm absorption bands of nitrate. J^* can be divided into contributions from each band

$$J^* = J^*_{200} + J^*_{305} = \Phi^*_{200}\int_{220}^{270} I(\lambda)\,\sigma(\lambda)\,d\lambda + \Phi^*_{305}\int_{270}^{400} I(\lambda)\,\sigma(\lambda)\,d\lambda. \quad (5)$$

Here, the depth dependencies of J^* and I were omitted for clarity and the quantum yield was assumed to be independent of λ.[15]

In order to distinguish the nitrate absorption bands experimentally, a UV filter with sigmoidal wavelength around 280 nm was used in one of two experiments (#7 and #8) of otherwise identical conditions, i.e., photolysis time, snow type, flow, etc. (see Table I). In principle, the experiment with the 280 nm filter (# 8) gives a value for J^*_{305} which corresponds to the second summand in Eq. (5), while the experiment with no filter gives J^* from both absorption bands. The UV filter also cuts off ~15% of the 305 nm band, as evaluated from the ratio of the photolysis rate constants (with and without the filter) above 270 nm. Φ^*_{200} can then be calculated from Eq. (5) as

$$\Phi^*_{200} = \frac{J^* - J^*_{305}}{\int_{220}^{270} I(\lambda)\,\sigma(\lambda)\,d\lambda} = \frac{J^*_7 - 1.15J^*_8}{\int_{220}^{270} I(\lambda)\,\sigma(\lambda)\,d\lambda}. \quad (6)$$

Here, subscripts 7 and 8 indicate experiment IDs and the factor of 1.15 accounts for the part of the 305 nm band cut off by the 280 nm filter. Φ^*_{200} is defined for the wavelength region 220–270 nm. The apparent quantum yield for the 305 nm band, Φ^*_{305}, is derived from Eqs. (4) and (5)

$$\Phi^*_{305} = \frac{J^* - J^*_{200}}{\int_{270}^{400} I(\lambda)\,\sigma(\lambda)\,d\lambda} = \frac{J^* - \Phi^*_{200}\int_{220}^{270} I(\lambda)\,\sigma(\lambda)\,d\lambda}{\int_{270}^{400} I(\lambda)\,\sigma(\lambda)\,d\lambda}. \quad (7)$$

TABLE I. Overview of experiments. The following properties are listed: snow type, starting nitrate mass fraction, average chloride, and sulfate mass fractions (all in ppbw = ng/g), photolysis time, t, UV filter sigmoidal wavelength, λ_{filter}, and gas flow, Q. All experiments were performed at −30 °C. Experiments 3, 7, 8, 9, and 10 correspond to experiments 6, 7, 8, 9, and 10 in Paper II.[41]

Exp #	Snow	$w_\circ(NO_3^-)$	$w(Cl^-)$	$w(SO_4^{2-})$	t /h	λ_{filter} /nm	Q /(l/min)	Comment
Test	Dome C	230.6	…	…	260	…	1.1	No light, SSA measurement
1	Dome C (2011)	1434.9	350.0	114.4	139.5	…	2.2	No light
2	Dome C (2009)	482.9	103.4	89.8	4.6	…	1.1	
3	Dome C (2011)	1731.0	436.0	86.3	20.3	…	1.1	
4	Dome C (2009)	466.4	86.1	87.1	88.2	…	1.1	
5	Dome C (2009)	503.2	97.9	76.8	114.4	…	1.1	Reverse flow direction
6	Dome C (2009)	421.1	131.9	95.9	137.8	…	1.1	Ice formation in light pathway
7	Dome C (2011)	1564.8	…	…	162.8	…	2.2	
8	Dome C (2011)	1433.9	368.7	102.1	164.0	280	2.2	
9	Dome C (2011)	1475.9	414.6	118.0	187.2	305	2.2	
10	Dome C (2011)	1519.4	434.3	158.4	283.2	320	2.2	

Φ^*_{305} is a function of depth, z, and will be reported in the remaining text as Φ^*.

D. Optical properties of snow and the Beer-Lambert law

Previous work has shown that the photon flux, I, changes nonlinearly with depth in a semi-infinite body of snow due to frequent scattering.[36] In a discussion of their Tropospheric Ultraviolet Visible (TUV) model, Lee-Taylor and Madronich[36] document two distinct zones characterized by the ratio of direct and diffuse light. Undisturbed sunlight has a large fraction of direct light resulting in an amplification of the photon flux just below the snow surface. Below that zone incoming light undergoes sufficient scattering in the snow, so that effectively all light becomes diffuse.

In the diffuse zone, the depth-profile of I can be fitted assuming a unique exponential decay for each wavelength. The exponential nature of the fit is based on the (modified) Beer-Lambert law

$$I(\lambda, z) = I_0(\lambda) \exp(-z/\eta(\lambda)), \tag{8}$$

where I_0 is the photon flux measured in the uppermost part of the diffuse zone in the snow and $\eta(\lambda)$ is the (exponential) fitting parameter known as the *e-folding depth* (written as $\eta(\lambda)$ to avoid confusion with the isotopic fractionation, ε). The quantity $\eta(\lambda)$ describes the depth at which 1/e of $I_0(\lambda)$ is remaining.

E. The Antarctic sunny day equivalent

In order to relate laboratory results to field studies, the exposure to nitrate-active photons is quantified. For this purpose, an actinometric quantity, the *Antarctic sunny day equivalent*, N_{asd}, is introduced. The idea is to illustrate the roles of the different nitrate photochemical domains and the importance of secondary chemistry as a function of absorbed photons under ambient conditions. Starting from the term in the denominator of Eq. (4) which describes the rate of photon absorption, the total number of photons absorbed by a sample in time t, N_{ph}, is given as

$$N_{\text{ph}}(z,t) = t \int_{\lambda>270} I(\lambda, z)\, \sigma(\lambda)\, \mathrm{d}\lambda = \frac{t\, J(z,t)}{\Phi(z,t)}. \tag{9}$$

N_{ph} is equivalent to the total number of excited nitrate molecules based on the liquid phase absorption cross section σ. The total number of absorbed photons can be calculated for an experimental sample, $N_{\text{ph}}^{\text{exp}}$, and for snow for a typical day in Antarctica, $N_{\text{ph}}^{\text{sun}}$, using the sun's actinic flux. It is assumed that the quantum yield for loss of nitrate determined in this study is applicable to the field in similar conditions. N_{asd} is defined as the ratio of absorbed photons, and Φ^* cancels

$$N_{\text{asd}} = \frac{N_{\text{ph}}^{\text{exp}}}{N_{\text{ph}}^{\text{sun}}} = \frac{t_{\text{exp}}\, J_{\text{exp}}}{0.5\, t_{\text{sun}}\, J_{\text{sun}}}. \tag{10}$$

J_{sun} is calculated from the modeled actinic flux at Dome C, cf. Figure 2, and the (arbitrary) factor of 0.5 accounts for variations in the actinic flux (e.g., clouds, changes in ozone column and solar zenith angle). A number of $N_{\text{ph}}^{\text{sun}} \approx 0.5$ is derived for $t_{\text{sun}} = 1$ d. A value of $N_{\text{asd}} = 1$ indicates that as many photons were absorbed by nitrate in the experiment as in one typical sunny day in Antarctica, hence the name.

III. METHODS AND MATERIAL

A. Snow

Two batches of snow from Dome C, Antarctica, were used in the experiments. The first batch was collected on 20 January 2009 ∼10 km South (S 75° 09′ 0″ E 123° 19′ 25″) of Concordia station (S 75° 06′ 00″ E 124° 33′ 29″). The snow can be considered to be from the clean area since it is collected upwind of the station. The first ∼10 cm of surface snow was sampled, homogenized, and placed in a thermally sealed double-walled polyethylene bag. Approximately 5 kg of snow were collected. The second batch was wind-blown snow sampled in the vicinity of Concordia station on 5 December 2011, when the wind was coming from the clean sector. The snow was stored until use at −25 °C in the dark.

The nitrate mass fraction on the day of collection was 570 ppbw for the 2009 batch and 1822 ppbw for the 2011

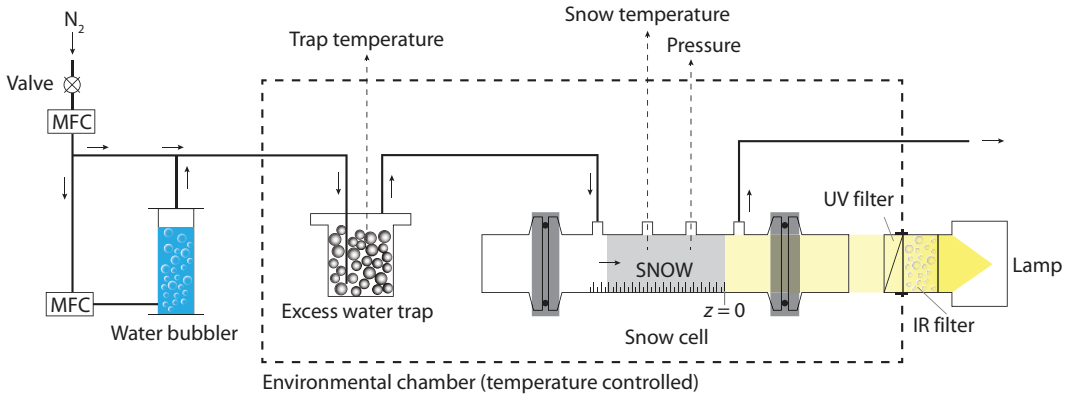

FIG. 3. Schematic drawing of the experimental setup and snow cell. The (∼400 ml) snow cell has UV transparent Suprasil windows and a printed scale on the outside to guide subsampling after experiments. It is placed, together with the excess water trap, inside a temperature controlled environmental chamber (dashed line). The Xe lamp, IR water filter, optional UV filters, and flow preparation setup are partly outside the environmental chamber, but are connected to the snow cell via ports. Pure nitrogen is provided from a liquid nitrogen tank. The flow direction is indicated by the small arrows and can be varied. MFC stands for mass flow controller.

batch. Comparison to the mass fractions prior to experiments of around 450 ppbw (2009 batch) and 1500 ppbw (2011), cf. Table I, indicates small changes during transport and storage due to denitrification by desorption of HNO_3.

All sample handling before and after the experiments was done in a cold room at LGGE at −15 °C. Inside the cold room, the snow was kept in the dark in insulated boxes. Before experiments the snow was homogenized by mechanical mixing to ensure a uniform nitrate distribution (both, in terms of concentration and its domain), in all experiments, and within each single experiment.

B. Experimental setup

Figure 3 shows an overview of the experiment. The cylindrical (∼400 ml) glass cell containing the snow consists of three parts which can be disassembled for filling: two ends with UV transparent Suprasil windows, and a center region where the snow is placed and which has four ports, for temperature and pressure readings, and in- and outflow of the water saturated nitrogen flow. The three parts are held together by metal clamps; sealing o-rings ensure that the closed cell is air tight. A scale was printed on the outside of the cell to guide subsampling after experiments. The snow cell is placed inside an environmental chamber of ∼1 m^3 volume which is temperature controlled via a PC interface. The chamber has ports which allow tubes and optical equipment to reach inside.

A Xenon arc lamp (300 W, LOT Oriel) is placed at one of those ports (outside the chamber), together with an infrared (IR) water filter to reduce the heat flux into the chamber, and a holder to place several optional UV filters to modulate the impinging light spectrum, cf. Figure 2 and Table I. The lamp was adjusted to be collimated at the snow column front, but due to the nature of the two arcs occurring within the lamp, the intensity of the beam was not completely uniform in a plane perpendicular to the optical axis. The snow cell was always placed in the same way relative to the fixed lamp, but small variations could not be avoided. Given the short distance between the lamp and the snow cell, no large changes in the spectrum due to absorption in air were observed.

Water-saturated nitrogen was flowed over the snow during experiments to remove photoproducts. Evaporated liquid nitrogen was used as carrier gas. A part of the N_2 flow was directed through a water bubbler in order to provide a water saturation of ∼150% for the set temperature of the environmental chamber and therefore the snow. The super-saturation takes the temperature difference between room and chamber (inside) into account. Since the water vapor pressure changes with temperature, the excess water is collected in a trap inside the chamber. After having been saturated with water vapor at the snow temperature, the flow passes through the snow in the glass cell and exits via a port. The flow direction can be changed. All tubes directing the flow are made of stainless steel, as is the excess water trap. The tubing for the pressure gauge and the exit line of the flow are made of Teflon. The temperature was measured using a thermocouple placed in a half-open ethanol-filled glass vial which was introduced into the snow column.

Prior to experiments, the gas line providing the saturated nitrogen flow was heated using a heat gun while flushing with nitrogen to remove any contaminants in the tubes. In between experiments, the nitrogen flow was kept above zero to prevent deposition and to sublimate any ice formed in the part of the gas line inside the chamber (including the excess water trap). The water in the bubbler was renewed regularly; tests of the water after several runs always showed nitrate concentrations below the detection limit.

C. Experimental procedure, sample treatment, and subsampling

A known mass of snow was homogenized and transferred into the pre-cleaned and cooled snow cell which had a Teflon sheet wrapped around its inside wall. This sheet ensures efficient removal of the snow after the experiment, as otherwise it sticks to the glass wall. The cell was filled vertically using a plunger which ensures a planar front (i.e., irradiated surface) and then closed and placed inside the pre-cooled

environmental chamber where all tubes and ports were connected. Once the temperature of the snow was stable, the experiment was started by flowing the conditioned stream through the snow and switching on the lamp.

The snow column is usually significantly hardened at the end of an experiment, so that it can be pushed out of the cell easily and sliced into pieces of ∼1 cm thickness using the scale on the cell. These slices are weighed individually in clean bags and then divided into two vials, one for ion concentration and one for isotopic measurements.[41] Sample vials were kept in insulated boxes in the dark in the same cold room until measurement.

D. Specific surface area (SSA) of the snow

Test runs without a lamp were performed to ensure the snow is not altered chemically or physically due to the flow system (e.g., desorption, crystal growth). Besides measuring nitrate concentrations as described below, the SSA of the snow was measured before and after the run. In order to do so, snow samples of the same batch which was used for the experiment were stored in LN_2 to make sure their properties do not change during storage. Also, after the experiments, a portion of the snow was stored in LN_2. The SSA was measured using the DUFISSS instrument (DUal Frequency Integrating Sphere for Snow SSA measurement) described elsewhere.[42,43] Briefly, DUFISS is based on the measurement of the hemispherical infrared reflectance of snow samples using a laser diode at 1310 nm, an integrating sphere, and InGaAs photodiodes. The instrument was calibrated using different reflectance standards prior to measurements. All SSA samples were analyzed at the same time to minimize variation. Samples were removed from the LN_2 dewar some hours before the measurement to allow the snow to equilibrate with the cold room's temperature.

E. Chemical and isotopic analysis

Ion chromatography (Metrohm) was used to measure the nitrate, sulfate, and chloride concentrations in each sample. Every set of ion chromatography measurements used freshly prepared standards and eluents.

The stable oxygen and nitrogen isotope ratios of nitrate were measured for each subsample. The results and discussion of this data are presented in Paper II.[41]

F. Optical characterization

An optical detection system consisting of a Maya2000PRO photo-spectrometer (wavelength region 220–400 nm), an optical fibre (solarized, 600 μm diameter), and a cosine corrector (CC-3-UV-T) was calibrated using a calibrated light source (DH-2000-CAL, all components Ocean Optics, Inc.) in order to measure absolute irradiances. Measurements were taken inside the snow column, comparable to Phillips and Simpson.[44] All spectra were corrected for dark noise, the integration times were varied depending on signal strength (up to the instrument maximum of 10 s) and spectra were averaged at least 10 times. A calibration using the DH-2000-CAL lamp was performed at room temperature. All measurements were performed in a walk-in cold room at −15 °C (the Xe lamp, snow cell, and photo-spectrometer were inside the cold room while the PC for data acquisition was kept outside). The manufacturer specified an uncertainty in the calibration spectrum of the calibrated light source of ±5%.

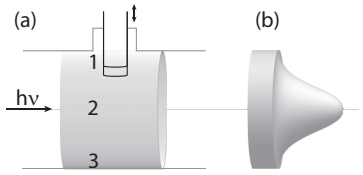

FIG. 4. Sketch of the irradiance measurement (a) and beam profile (b) inside the snow column. The optical fibre was inserted in the snow using one of the ports of the snow cell. Measurements were taken at positions 1, 2, and 3. The beam profile illustrates the assumed spatial (Gaussian) distribution of the photon flux inside one disk/subsample of the column (indicated in (a) by the grey cylinder). The photon flux is non-zero at the edges (positions 1 and 3).

Figure 4 shows how the absolute irradiance of the Xe lamp was recorded inside the snow column. The optical fibre and cosine corrector were placed at the same depths as for the subsampling using one of the snow cell's ports. The fibre was placed radially at three positions per depth step, see Figure 4 for details. The snow column was refilled at each depth using the same snow (from Dome C) as for the photolysis experiments.

The absolute (Xe lamp) irradiances measured in the snow at positions 1, 2, and 3 (shown in Figure 4) were converted to total photon fluxes in each layer as follows. First, the field of view of the cosine corrector was taken to be 120° based on its geometry. All measured irradiances were corrected accordingly. Irradiances measured at positions 1 and 3 were added, and the data from position 2 doubled, in order to account for the full field of view at both the edge and the center of the snow column. This approximation is valid because snow is highly scattering, i.e., major parts of the radiation along the optical axis are well represented and not excluded, as was tested by longitudinal measurements. As a second approximation, a circular, Gaussian distribution of the photon flux in the base plane of the disk was assumed. Note that the photon flux obtained using this method is non-zero at the edge, equivalent to a disc-shaped offset of the Gaussian beam profile ((b) in Figure 4). Finally, the average of the derived profile is taken as the photon flux at that specific depth, $I(\lambda, z)$.

This set of data, later denoted as "Xe lamp irradiances," was used to determine the complete photon flux inside the snow column. Another set of measurements was taken placing the fibre in position 2 of the first subsample and recording one spectrum per UV filter, labeled "filter irradiances" below. Together with the first data set, the photon flux in the total column was derived for each UV filter.

The Xe lamp irradiances are fitted using Beer-Lambert's law (Eq. (8)), where $I_0 = I(z = 1\,\text{cm})$ is the photon flux 1 cm into the snow. The reference point was chosen to be inside the snow since the front of the snow column reflects a

significant portion of the emission of the Xe lamp due to the snow's very high albedo. The resulting set of $\eta(\lambda)$ describes the optical properties of the snow cell. For further data processing, an exponential fit at each wavelength was used to construct a *synthetic* profile of the photon flux based on the measured value at $z = 1$ cm. Similarly, the filter irradiances measured at $z = 1$ cm are used to reconstruct the filtered photon flux at all depths inside the snow cell. In other words, Eq. (8) is also used to derive $I(\lambda, z)$ for the filtered cases, using the same $\eta(\lambda)$ and $I_0(\lambda)$ for the filtered cases. This parametrization allows accurate modeling of the photon flux for each UV filter.

Using the synthetic instead of the measured photon flux and assuming a Gaussian beam profile reduces uncertainties in the measurements. Besides, the uncertainty in the calibration spectrum uncertainties include: (i) The measurement method is intrusive which might allow some photons in the column to be absorbed by the fibre and cosine corrector without being detected, (ii) variations in the placement of the filled snow cell with the probe installed relative to the lamp (angle and side ways) changed the signal within a range of 20 %, (iii) placement of the probes inside the snow was accurate to within ±1 mm, both radially and laterally, (iv) the difference in temperatures between the photolysis experiments (−30 °C) and the photon flux measurements (−15 °C), (v) the distance between the lamp and the snow cell was accurate to within ±1 cm; given the low atmospheric absorption in the wavelength region of interest, this plays a minor role.

Table I gives an overview of the experiments presented in this paper. All experiments were conducted using a 300 W Xenon lamp and at −30 °C. The total flow of nitrogen, Q, and the duration of irradiation, t, were varied; the photon flux was changed using UV filters.

IV. RESULTS

A. Snow mass

The masses of the subsamples, weighed after experiments, differed only slightly, ensuring that the results are comparable to each other. Sample masses were nominally 15 g and the standard deviation of the sample masses was less than 1 g ($n = 8$). The total snow mass weighed before and after photolysis typically differed by less than 1%.

B. Photon flux and e-folding depths

Figure 5 shows the profile of the photon flux as a function of wavelength and depth in the snow column. The amplification in the first couple of millimeters, predicted for low solar zenith angles by TUV models,[36,38] is not observed. This might be because of the low depth-resolution of the measurements, or the non-semi-infinite geometry of the setup.

At a distance of 5 or 6 cm into the snow, the photon flux decreases more than 10-fold (Figure 5); photolysis deeper in the snow is disregarded as the signal-to-noise ratio decreases accordingly. Equation (4) assumes that the measured photon flux is the same in all experiments. As noted in Table I experiment #6 had ice accumulating in the light path over time due

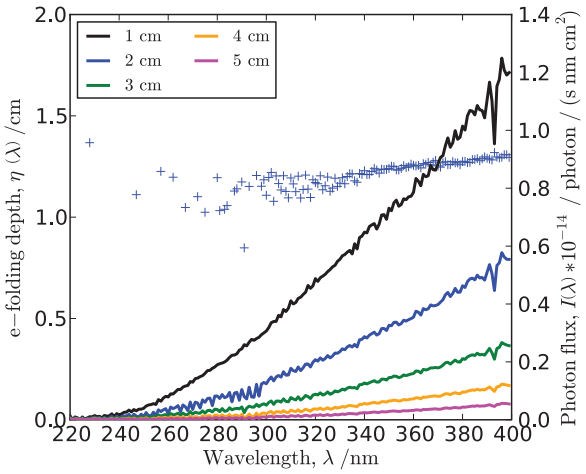

FIG. 5. e-folding depths, $\eta(\lambda)$, (crosses, left axis) and photon fluxes measured without UV filter at different depths, z, as given in the legend (lines, right axis). 1/e of the incoming light is remaining at shallow depth (∼1 cm). Values of $\eta(\lambda)$ are only given when the exponential fit of the photon fluxes over depth fulfilled $R^2 > 0.9$, eliminating noisy data below 300 nm.

to humid ambient conditions. This, considered together with other potential issues concerning the measurement technique itself means that the photon flux results are a lower limit, since the method is unlikely to measure more photons than are present.

Figure 5 also shows the e-folding depths, $\eta(\lambda)$, as a function of wavelength. Only those values are given for which the fit fulfilled $R^2 > 0.9$, a condition usually not met below 300 nm due to the low photon fluxes, cf. Figure 5. The e-folding depth was observed to be $\eta(\lambda) \approx 1.2$ cm and rather independent of λ. This is significantly lower than reported in ambient measurements (by a factor of 5–20[19,45]), probably due to the non-semi-infinite boundary conditions given by the glass cell.

C. Physical properties of snow and SSA

The SSA did not change significantly over the course of dark experiments in which there is flow but no light present (data not shown). It can therefore be assumed that the snow did not change due to storage and handling or flow. When handling the snow after photolysis experiments, changes in the front part of the snow were apparent, with notably more hardening for longer experiments. Due to the small amounts of snow available, the change in SSA could not be measured using DUFISS. Therefore, no quantification of the metamorphism is available but they most likely stem from absorption of light. The SSA is expected to decrease with time.

D. Nitrate loss and photolysis rate constants

Figure 6 shows the mass fractions of NO_3^-, Cl^-, and SO_4^{2-} in experiment # 4 before and after irradiation. For these ions only nitrate is affected with its concentration decreasing in the first 6 cm of the snow column.

Figure 7 shows the nitrate fraction remaining in the snow after photolysis for all experiments. The experiment in the dark with gas flowing (#1) showed no change in the nitrate concentration. Besides being a successful blank test, this

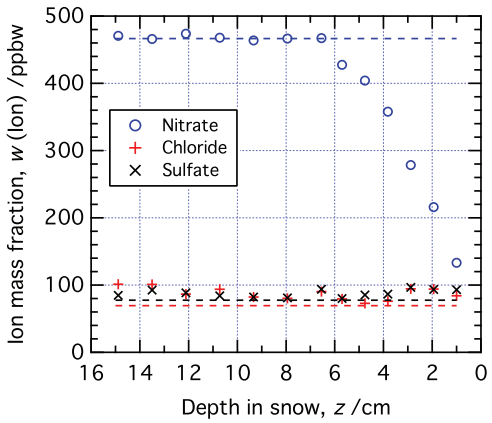

FIG. 6. Ion concentration profile in the snow after ~86 h of irradiation (experiment #4). The single data points each represent one subsample of approximately 1 cm thickness starting from the surface. The dashed lines indicate the respective ion concentrations of the initial snow prior to irradiation.

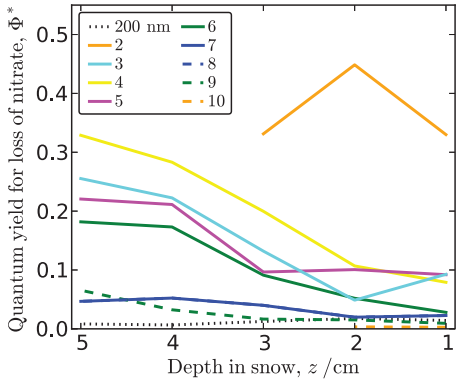

FIG. 8. The quantum yield for loss of nitrate due to the 305 nm band, Φ^*, as determined for different experiments (numbers in legend) without UV filter (full lines) and with UV filters (dashed lines) as a function of depth in snow. Experiments #7 and #8 have the same values due to the applied corrections (see text for details). The apparent quantum yield for the 200 nm band is also given (dotted line). See Table I for experimental details.

strongly suggests that no nitrate desorbed off the snow into the water-saturated flow of nitrogen. All the other experiments show a loss of nitrate in the first couple of centimeters in the snow, independent of flow magnitude and direction. Depending on the length of UV exposure (photolysis time), nitrate losses occur within the first 6 cm of snow.

V. DISCUSSION

A. Desorption-free photolysis system with recombination

As the nitrate concentration and SSA did not change in experiments with no light present, it is safe to assume that photolysis is the main loss process acting in experiments with the light turned on. In particular, desorption was shown to play no role in the blank experiments. Also, the unchanged snow mass before and after experiments shows that there was no change due to sublimation or condensation. The Cl^- and SO_4^{2-} ion concentrations show that no macroscopic transport of water is present even after long photolysis times and that contamination (e.g., from NaCl) is low. However, the physical properties of the snow did change with the light source

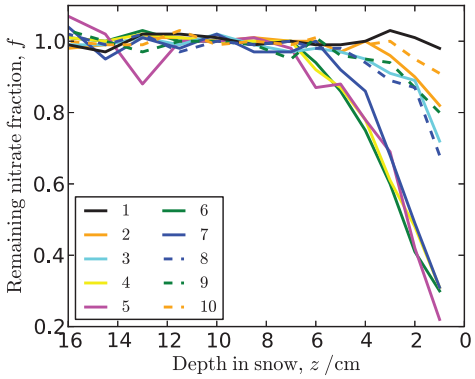

FIG. 7. The measured remaining nitrate fraction in the snow after UV exposure. Numbers in the legend correspond to experiment numbers in Table I. Depending on the photolysis time, nitrate is lost up to 6 cm depth. Experiment #2 only shows losses in the first 3 cm and experiment #10 only in the first 2 cm.

switched on and snow metamorphism could in principle make nitrate more available for evaporation. Given the lower loss rates observed at longer photolysis times (see below), desorption does not seem to play a major role under any conditions. In contrast, the production of nitrate via recombination of photolysis products may explain decreasing apparent photolysis rate constants.

B. Superposition of two domains of snow photochemistry

Figure 8 shows the apparent quantum yields derived by relating the predicted number of absorbed photons (derived from the photon flux measurement) to the apparent photolysis rate constants (derived from the measured nitrate concentrations) for different experimental conditions (Eq. (4)). All values lie below 0.5 and span a wide range extending to 0.003. Two trends are visible: first, the apparent quantum yield increases with increasing z, and second, the apparent quantum yield decreases with photolysis time (the shortest experiment, #2, has the highest values of Φ^*). The changes in apparent quantum yield exceed the measurement error of the irradiances. For instance, in experiment # 3, Φ^* changes by a factor larger than 3 compared to an error of 20%–30% in the optical measurement which is smoothed by the fitting procedure. More specifically, the measured photon flux was regarded earlier as an upper limit and therefore the reported quantum yield for loss of nitrate is a lower limit.

One origin of the depth dependence of the apparent quantum yield is the secondary chemistry terms A and B in the mass-balance equation (Eq. (1)). Considering that photolysis yields both NO_x and the radicals that oxidize it to reform nitrate, nitrate reformation will have a nonlinear dependence on light intensity. This is consistent with the lower measured apparent quantum yield at the top of the column (Figure 8). However, it seems that secondary chemistry alone is not able to explain the observed time dependence: the short experiment #2 yielded a high apparent quantum yield at low depths where nitrate was exposed to a high photon flux.

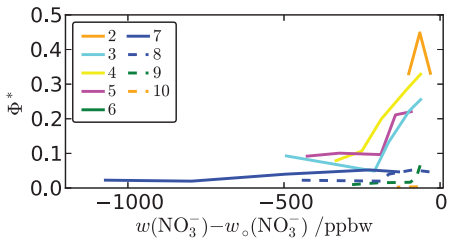

FIG. 9. The quantum yield for loss of nitrate as a function of change of nitrate mass fraction for different experiments (numbers in legend, see Table I for details). Nitrate photolysed initially shows higher apparent quantum yields than nitrate lost later.

In contrast, both trends can be explained by the superposition of photochemical domains of nitrate in snow. Considering a system with two such domains, one of photolabile and one of buried nitrate, the former would give a larger apparent quantum yield while the latter will have a smaller apparent quantum yield. Figure 9 shows that nitrate lost initially is photolabile and only after bleaching this domain, buried nitrate will get photolysed too. Translated to the depth and time dependence this means that in the first hours of the experiment, nitrate is easily photolysed in the front of the snow column. During longer experiments the snow in the back (below 3 cm) is also exposed to significant amounts of UV radiation, similarly photolysing easily accessible nitrate (hence giving large values of Φ^*). In the front, the buried nitrate is not photolysed as easily anymore. Over time the curve of the quantum yield for loss of nitrate shifts to the left in the representation of Figure 8.

It is likely that the values of Φ^* close to 0.25 relate to the photolysis of photolabile nitrate, while the value of $\Phi^* \approx 0.05$ corresponds to photolysis of buried nitrate with a stronger contribution from secondary (recombination) chemistry. The finding of non-constant quantum yields is in line with results of similar experiments in the literature that suggest two photochemical reservoirs of nitrate[18,20,30] – with one more prone to nitrate dissociation – and experiments that show changing photolysis rates.[27,29]

The highest apparent quantum yields are close to the value of Zhu *et al.*[16] Therefore, it seems likely that samples with such high apparent quantum yields experienced similar conditions as in this reference where HNO_3 was adsorbed on ice.

The lower apparent quantum yields are close to Chu *et al.*'s.[15] In order to explain them, a simplified picture of nitric acid solvation (i.e., ignoring other ions) is considered here. The phase diagram[46] suggests that the experimental conditions of the present study fall either into a solid solution of HNO_3 in ice or into a metastable phase where aqueous HNO_3 solutions and solid solutions of HNO_3 in ice coexist. In this framework, the experiments by Chu and Anastasio[15] were performed exclusively in the same metastable phase. The partitioning coefficient between solid and liquid phases[46] is $\sim 10^{-6}$ for -30 °C and indicates that most nitrate is in the liquid phase in the case of Chu and Anastasio.[15] In the liquid phase, nitrate is exposed to surrounding water molecules and a strong cage effect.[26] Chu and Anastasio[15] argue that nitrate is photolysed in the DI in their experiments. The difference between solid solution, DI, and aqueous solution is not resolved in the present study, but it is suggested that whichever domain is the dominant one has a small apparent quantum yield. A nitrate domain not present in the Chu and Anastasio[15] study is distinguishable due to its higher apparent quantum yield.

The snow used in this study shows nitrate in multiple domains, while the adsorption of HNO_3 resulted predominantly in photolabile nitrate in the work of Zhu *et al.*[16] and the freezing of an aqueous solution created mostly buried nitrate in the study of Chu and Anastasio.[15] The quantum yields found in these studies are a direct result of the specific preparation method used. Because such artificial conditions are not expected to be met fully in the present study or at Dome C, the apparent quantum yields reported here are not equal to the ones reported by the other groups. Instead, the apparent quantum yield is always larger than the one by Chu and Anastasio[15] and always smaller than the one by Zhu *et al.*[16]

Given the absorption cross section for adsorbed nitrate, the photochemistry of both domains could be discussed individually and eventually included in models. Since Zhu *et al.*[16] determined the absorption cross section of adsorbed nitrate only at a single point (308 nm) such a description is not possible at the moment. The presented apparent quantum yield therefore incorporates potential enhancements in the cross sections of photolabile species.

The experimental results show the significant role of nitrate de-excitation and reformation in snow photochemistry. However, the measured quantum yield does not depend on light intensity alone, disproving the first hypothesis in the introduction. Instead, reformation of nitrate has to be viewed in the context of the domain of nitrate snow photochemistry which is consistent with the second hypothesis. The experimental results support attribution of the two literature values of the apparent quantum yield[15,16] to the photolysis of different nitrate pools.

C. Application to UV exposures at Dome C

Figure 10 shows the quantum yield for loss of nitrate as a function of Antarctic sunny day equivalents for all experiments and shows different snow batches with different symbols. In this visualization, the depth and time dependence of Φ^* is a function of one single variable which is equivalent to UV exposure. An exponential fit describes the decline in the apparent quantum yield well, cf. Table II. The change in apparent quantum yield suggests that after exposure to enough photons all photolabile nitrate has been photolysed and the pool of buried nitrate becomes more prominent, making secondary reaction pathways more important. An arbitrary cutoff quantum yield of $\Phi^* = 0.12$ was chosen based on Figure 10 to distinguish the two nitrate domains. Table III shows that the average apparent quantum yield is five times larger in the photolabile domain than it is in the buried domain, while the lifetime of nitrate in snow, $\tau = 1/J^*$, decreases by a factor of 2.7. Nitrate lifetimes of ~1–2 weeks are in line with characteristic lifetimes for nitrate in summer in Dome C (~2 weeks[37,47]).

As indicated by the fitting curves in Figure 10, the two different batches of snow require different lengths of time

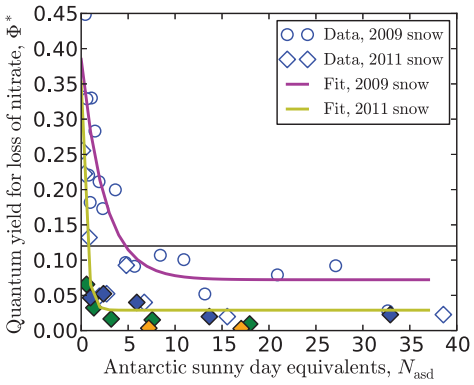

FIG. 10. The quantum yield for loss of nitrate, Φ^*, as a function of Antarctic sunny day equivalents, N_{asd}. Same data as in Figure 8 with colored diamonds for data from experiments # 8 (blue), # 9 (green), and # 10 (orange). Antarctic sunny day equivalents provide a metric of UV exposure to relate the findings of this study to ambient measurements ($N_{asd} = 1$ corresponds roughly to the number of photons absorbed by nitrate in one sunny day in Dome C). The exponential nature of the fit was chosen arbitrarily (cf. Table II). The black line indicates an arbitrarily chosen cutoff at $\Phi^* = 0.12$ that distinguishes the nitrate domains (cf. Table III).

before the lower limit of the apparent quantum yield is reached. While the apparent quantum yield levels off over the course of a week in the 2009 snow, it only needs a couple of days in the 2011 (wind-blown) snow to bleach the photoactive nitrate. In the terminology used in this study, this indicates that the 2011 snow has a larger fraction of buried nitrate than the 2009 batch. This may seem counterintuitive: the 2011 batch is drifted snow with a potentially large fraction of surface adsorbed HNO_3 from recycling of reactive nitrogen that could be associated with photolabile nitrate and the smaller nitrate fraction of the 2009 batch indicates previous processing and hints at buried nitrate remaining. However, the local domain of nitrate might be influenced by many factors, including, for example, the much higher chloride concentrations in the 2011 wind blown snow than in the 2009 batch, cf. Table I.[48]

D. The 200 nm absorption band of nitrate

The quantum yield for loss of nitrate from the 200 nm band, Φ^*_{200}, was found to be 0.012 ± 0.004 (1−σ) in the first 5 cm of snow which is small but leads to significant nitrate loss given the strength of the 200 nm band. Even though the quality of the photon flux data below 300 nm declines (Figure 5), Φ^*_{200} is an upper limit because photons emitted by the Xe lamp below 220 nm were not detected. Since Φ^*_{200} resembles the 220–270 nm region, the value of 0.01 is much

TABLE II. Determined values and parametrization of the quantum yield for loss of nitrate in snow, Φ^*.

Data	min (N_{asd})	max (N_{asd})	Mean	p_0, p_1, p_2, p_3[a]
2009	0.028 (33)	0.44 (0.5)	0.19	0.07, 19.0, −10.3, 2.5
2011	0.003 (17)	0.26 (0.1)	0.06	0.03, 25.8, −2.0, 0.5
All	0.003 (17)	0.44 (0.5)	0.12	0.05, 23.1, −6.1, 1.4

[a]Fitting function: $p_0 + p_1 \exp(-(x - p_2)/p_3)$.

TABLE III. Quantum yield for loss of nitrate in snow and mean lifetime for different nitrate domains using an arbitrary cutoff at $\Phi^* = 0.12$.

Domain	min (N_{asd})	max (N_{asd})	Mean	τ /d
Buried	0.003 (17)	0.12	0.05	16.3
Photolabile	0.12	0.45 (0.5)	0.26	6.1

lower than what Goldstein and Rabani[49] reported at any wavelength in that region. In the present study, the loss of nitrate is suppressed in the 200 nm band and enhanced in the 305 nm band compared to the aqueous phase. While the effect of parameters like the photochemical domain or temperature is even more elusive for the 200 nm band than for the 305 nm band, our results could suggest that the additional isomerization pathway in the 200 nm band leads to more reformation of nitrate when comparing photolysis in snow to the liquid phase. The large photolysis rates in the 200 nm band also enhance product species concentrations that might promote reactant reformation within the snow matrix.

The cutoff wavelength used in this study to distinguish both bands (270 nm, Eq. (5)) allows only for a minor contribution of the 200 nm band to the magnitude of reported results of Φ^*_{305}. There is however the theoretical possibility that the 200 nm band causes some of the observed dynamics in the quantum yields. Based on the present dataset this cannot be discussed further, but other studies that reported changes in photolysis rates in snow (without $\lambda < 300$ nm present)[27,29] support the attribution of such dynamics to the 305 nm band.

E. Nitrate concentrations and NO_x production at Dome C

Nitrate concentrations in snow measured in 2007 at Dome C[11] showed mass fractions of 330 ng/g in the top layer decreasing to 30 ng/g at 50 cm depth. The concentration profile is very steep in the first 5 cm, after which only 50 ng/g of nitrate remains. Light penetrates several tens of cm at Dome C[19] and the nitrate left at such depths can be assumed to be buried, associated with smaller values of Φ^*. Nitrate is replenished at the top by fresh snow layers and by dry-deposited nitrate, both of which can be assumed to be rather photolabile and therefore to be associated with large apparent quantum yields.

The quantum yield for nitrate photolysis is usually assumed to be constant, so that in a simple approach the quantum yield for loss of nitrate can be applied directly to the conditions of interest (nitrate concentration profile, snow type, etc.) by replacing Φ_{OH} by Φ^* in the flux calculations. The apparent quantum yields found in the present study exceed $\Phi_{OH} = 0.0019$ – the quantum yield that typically estimates day-time NO_x emission from the snow pack at −30 °C correctly[13,15,19] – by factors of $\frac{\Phi_{OH}}{\Phi^*} \approx$ 2–230. The day-time NO_x fluxes are therefore over-predicted by the same range of factors. For example, the average of all apparent quantum yields ($\Phi^* = 0.12$, Table II) over-predicts NO_x fluxes by a factor of ∼60. A number of constrains come with such simplified estimates.

The over-prediction of NO_x fluxes hints at other chemical or physical processes in the snowpack that moderate the effect of the larger quantum yields on predicted NO_x fluxes. The recombination of NO_x photoproducts to form nitrate before leaving the snow is such a candidate and in the field recombination might prevent NO_x from being detected above ground despite potentially large photolysis rates in the snow. The present setup was designed to minimize recombination during a typical 100 h experiment by flushing ∼6000 l N_2 over the snow. Given a cell volume of 400 ml, all generated NO_x will be too diluted to provide meaningful nitrate recombination rates.

Validating quantum yields using measured NO_x fluxes is also prone to other issues including nitrogen species that are omitted during such measurements (e.g., HONO, HO_2NO_2, N_2O_4). A potentially very short lifetime of NO_x in the first cm above the snow may also lead to conversion of NO_x before detection by an instrument that is located several tens of meters away from the inlet.

The NO_x emission model by Frey *et al.*[13] over-predicted the ratio between day time and night time NO_x fluxes. Based on the presented results this ratio qualitatively decreases by assuming a 2-layer system, where surface snow has a high and snow deeper down has a low quantum yield (the latter seeing no light at night). Night time NO_x flux is high, but increases relatively less during daytime when compared to the standard case where the quantum yield is constant at all depths.[13] Frey *et al.*[13] mention the deposition of NO_x photoproducts within the snowpack as one of the main uncertainties in their model. Such a process reduces NO_x fluxes above the snow pack and needs further investigation in order to be parametrized for inclusion in models.

VI. CONCLUSIONS

The photolysis of nitrate was investigated using natural snow in a temperature controlled chamber. The experiments show no desorption of nitrate, while providing a constant gas flow to prevent the deposition of recombined gas-phase products. Two batches of snow, sampled at Dome C, Antarctica, were used. They ensure similar microphysical locations of nitrate in the experiment and field (neglecting effects of transport and storage). Both the photon flux and the nitrate concentration were measured inside the snow to derive an apparent quantum yield for loss of nitrate, Φ^*, which takes secondary chemistry and the photochemical domain into account. The derived values lie between 0.44 and 0.003 – well within the range of those reported previously (0.6 at −20 °C by Zhu *et al.*[16] and 0.0019 at −30 °C by Chu and Anastasio[15]).

The decrease of the apparent quantum yield with UV exposure is discussed here as arising from the superposition of two domains of nitrate in snow photochemistry: photolabile and buried. It is suggested that the very different quantum yields found in the literature can be viewed as limiting values of photolysis of photolabile nitrate (large Φ^*) and the photolysis of buried nitrate (small Φ^*). Photolabile nitrate might correspond to what other authors called surface/adsorbed nitrate and gives rise to a higher apparent quantum yield because reaction products can leave the snow easily. The behavior of buried nitrate might resemble that of nitrate in aqueous solution, bulk ice or the DI. Here, the escape of products is inhibited by the cage effect and an enhanced role of secondary (e.g., recombination) chemistry. Buried nitrate is less sensitive to flow and results in a much lower apparent quantum yield. The corresponding lifetimes of nitrate, $\tau = 1/J^*$, are 6 and 16 days for the photolabile and buried domains.

Nitrate concentrations in snow and the actinic flux have been measured in field and modeling studies.[19,50] Such studies often assume a single, unidirectional photolysis reaction of nitrate with a constant quantum yield in order to predict NO_x emissions out of the snow. They therefore ignore secondary chemistry and the different active domains of nitrate. This study suggests that the commonly used quantum yield is insufficient in reproducing this complex mechanism. The Antarctic sunny day equivalent, N_{asd}, metric was introduced for intercomparison of laboratory and field studies. The results of this study help to decrease the difference between modeled night and daytime NO_x emissions but lead to an over prediction of NO_x fluxes.

Paper II[41] discusses the stable oxygen and nitrogen isotope ratios of nitrate of the same samples as in this study. By using snow from Dome C, both papers provide the input needed for refined models to reproduce isotopic data measured in Dome C ice cores.

ACKNOWLEDGMENTS

The research has received funding from the European Community's Seventh Framework Programme (FP7/2007-2013) under Grant Agreement No. 237890 (J.S., T.A.B., C.M., and M.S.J.). C.M. and M.S.J. thank the University of Copenhagen for supporting this research. J.S. and T.A.B. gratefully acknowledge The Agence Nationale de la Recherche (ANR) for its financial support through the OPALE project (Contract No. NT09-451281). LEFE-CHAT, a scientific program of the Institut National des Sciences de l'Univers (INSU/CNRS), provided partial funding for this study (J.S., T.A.B., and J.E.). J.S., T.A.B., and J.E. acknowledge IPEV for providing access to Concordia station through funding the SUNITEDC program (1011). J.S. has been supported by a grant from Labex OSUG@2020 (Investissements d'avenir - ANR10 LABX56). J.S., T.A.B., C.M., and M.S.J. also thank IntraMIF. SSA measurements were performed together with Florent Domine, LGGE, now at Takuvik Joint International Laboratory, Université Laval (Canada) and Samuel Morin, Météo-France/CNRS, CNRM-GAME, Centre d'Etudes de la Neige / Snow Research Center. C.M. thanks Julia Lee-Taylor for her assistance with the TUV model.

APPENDIX: DETAILED REACTION MECHANISM

The complete reaction mechanism of nitrate photolysis as shown in Figure 1 is described here. The main excitation in ambient environments is

$$NO_3^- + h\nu \xrightarrow{\lambda > 300\,nm} [NO_3^-]^{n\pi^*}. \quad (A1)$$

The product is an excited state of the nitrate ion resulting from an $\pi^* \leftarrow$ n transition, abbreviated as $n\pi^*$, Ref. 51. The square brackets denote solvent cages. The excited $n\pi^*$ nitrate can undergo several reaction pathways, one of them being the back reaction which is promoted by the solvent cage

$$[NO_3^-]^{n\pi^*} \rightarrow NO_3^-. \quad (A2)$$

The main forward reaction gives NO_2

$$[NO_3^-]^{n\pi^*} \xrightarrow{H^+} NO_2 + OH. \quad (A3)$$

Another forward reaction is less likely (1 out of 9, Ref. 52) but forms the important nitrite ion

$$[NO_3^-]^{n\pi^*} \rightarrow NO_2^- + O. \quad (A4)$$

Secondary chemistry (thin lines in Figure 1) is described next, starting with nitrite photolysis

$$NO_2 + h\nu \rightarrow NO + O^- \quad (A5)$$

and nitrite protonation giving HONO ($pK_a = 3.2$)

$$NO_2^- + H^+ \rightarrow HONO. \quad (A6)$$

The O^- product from reaction (A5) readily forms the OH radical ($pK_a = 11.9$), while the NO product can leave the system as a gas or undergo further reaction, such as reaction with OH

$$NO + OH \rightarrow HONO. \quad (A7)$$

NO_2 may undergo additional reactions

$$2NO_2 + H_2O \rightarrow NO_2^- + NO_3^- + 2H^+ \quad (A8)$$

with back reaction

$$NO_2^- + OH \rightarrow NO_2 + OH^-. \quad (A9)$$

Another way to form HONO is

$$NO_2 + NO + H_2O \rightarrow 2HONO. \quad (A10)$$

And finally another way to reform nitrate

$$NO_2^- + OH \rightarrow HOONO \rightarrow NO_3^- + H^+. \quad (A11)$$

Secondary chemistry as in reactions (A5)–(A11) might depend on light intensity, as these reactions require two photoproducts to react with each other. These reactions may play a larger role in the case of buried compounds, e.g., after long photolysis times when the photolabile nitrate has been removed. The described secondary chemistry may reform nitrate and is indicated by the A and B terms in Figure 1.

The generation of reactive species from other chromophores might also play a role in nitrate photolysis in natural snow. For example, the photolysis of gas-phase NO_2 and HONO are not considered in the reaction mechanism explicitly, but may act as mechanisms to recover NO and produce OH. Similarly, the photolysis of H_2O_2 and organic compounds can be considered as a source of OH. Given the high purity of Dome C snow and the flushing of the experimental cell, other chromophores are not believed to play a significant role in the present study. However, species other than nitrate dominate light absorption and this might alter the photochemistry of nitrate, e.g., via produced OH radicals that can oxidise nitrate.

Chemical reaction following UV absorption by nitrate at wavelengths below 300 nm is indicated in blue in Figure 1. This pathway is initiated by the following excitation:

$$NO_3^- + h\nu \xrightarrow{\lambda<300\,nm} [NO_3^-]^{\pi\pi^*}. \quad (A12)$$

Note the different excitation from a $\pi^* \leftarrow \pi$ transition indicated by $\pi\pi^*$. Madsen and co-workers[51] showed that nearly half of the excited nitrate decays into the ground state

$$[NO_3^-]^{\pi\pi^*} \rightarrow NO_3^-. \quad (A13)$$

The other half forms peroxynitrite, $ONOO^-$, Ref. 51

$$[NO_3^-]^{\pi\pi^*} \rightarrow ONOO^-. \quad (A14)$$

And only a small portion (8%) decays in a third channel

$$[NO_3^-]^{\pi\pi^*} \rightarrow (NO + O_2)^-. \quad (A15)$$

Here, the brackets are adopted from Ref. 51 since the negative charge could not be specifically assigned to either of the products. Peroxynitrite, $ONOO^-$, can isomerize back to nitrate or form the same species as in (A15)

$$ONOO^- \rightleftharpoons (NO + O_2)^-. \quad (A16)$$

NO and O_2 can react further to give NO_2 and nitrite via peroxynitrite[49] as indicated in the last reaction

$$(NO + O_2)^- \rightarrow \ldots \rightarrow NO_2 \text{ and } NO_2^-. \quad (A17)$$

NO_2 and nitrite can participate in the cycles (A and B) shown in Figure 1 the same way as if formed via the 305 nm band excitation. In the aqueous phase, the quantum yields of the channels (A14)–(A17) are wavelength dependent,[49] with their sum falling from ~0.5 at 220 nm to <0.01 at 300 nm.

[1] J. H. Seinfeld and S. N. Pandis, *Atmospheric Chemistry and Physics: From Air Pollution to Climate Change*, 2nd ed. (Wiley, Hoboken, 2006), p. 209.
[2] J. N. Galloway, F. J. Dentener, D. G. Capone, E. W. Boyer, R. W. Howarth, S. P. Seitzinger, G. P. Asner, C. C. Cleveland, P. A. Green, E. A. Holland *et al.*, Biogeochemistry **70**, 153 (2004).
[3] A. R. Ravishankara, J. S. Daniel, and R. W. Portmann, Science **326**, 123 (2009).
[4] J. E. Dibb, R. W. Talbot, J. W. Munger, D. J. Jacob, and S.-M. Fan, J. Geophys. Res. **103**, 3475, doi:10.1029/97JD03132 (1998).
[5] M. G. Hastings, E. J. Steig, and D. M. Sigman, J. Geophys. Res. **109**, D20306, doi:10.1029/2004JD004991 (2004).
[6] J. N. Galloway, A. R. Townsend, J. W. Erisman, M. Bekunda, Z. Cai, J. R. Freney, L. A. Martinelli, S. P. Seitzinger, and M. A. Sutton, Science **320**, 889 (2008).
[7] D. L. Fibiger, M. G. Hastings, J. E. Dibb, and L. G. Huey, Geophys. Res. Lett. **40**, 3484, doi:10.1002/grl.50659 (2013).
[8] P. Wagnon, R. J. Delmas, and M. Legrand, J. Geophys. Res. **104**, 3423, doi:10.1029/98JD02855 (1999).
[9] R. Röthlisberger, M. A. Hutterli, S. Sommer, E. W. Wolff, and R. Mulvaney, J. Geophys. Res. **105**, 20565, doi:10.1029/2000JD900264 (2000).
[10] R. Röthlisberger, M. A. Hutterli, E. W. Wolff, R. Mulvaney, H. Fischer, M. Bigler, K. Goto-Azuma, M. E. Hansson, U. Ruth, M. L. Siggaard-Andersen, and J. P. Steffensen, Ann. Glaciol. **35**, 209 (2002).
[11] M. M. Frey, J. Savarino, S. Morin, J. Erbland, and J. M. F. Martins, Atmos. Chem. Phys. **9**, 8681 (2009).
[12] R. E. Honrath, Y. Lu, M. C. Peterson, J. E. Dibb, M. A. Arsenault, N. J. Cullen, and K. Steffen, Atmos. Environ. **36**, 2629 (2002).
[13] M. M. Frey, N. Brough, J. L. France, P. S. Anderson, O. Traulle, M. D. King, A. E. Jones, E. W. Wolff, and J. Savarino, Atmos. Chem. Phys. **13**, 3045 (2013).
[14] R. E. Honrath, S. Guo, M. C. Peterson, M. P. Dziobak, J. E. Dibb, and M. A. Arsenault, J. Geophys. Res. **105**, 24183, doi:10.1029/2000JD900361 (2000).

[15]L. Chu and C. Anastasio, J. Phys. Chem. A **107**, 9594 (2003).
[16]C. Zhu, B. Xiang, L. T. Chu, and L. Zhu, J. Phys. Chem. A **114**, 2561 (2010).
[17]T. Bartels-Rausch, H.-W. Jacobi, T. F. Kahan, J. L. Thomas, E. S. Thomson, J. P. D. Abbatt, M. Ammann, J. R. Blackford, H. Bluhm, C. Boxe, F. Domine, M. M. Frey, I. Gladich, M. I. Guzmán, D. Heger, T. Huthwelker, P. Klán, W. F. Kuhs, M. H. Kuo, S. Maus, S. G. Moussa, V. F. McNeill, J. T. Newberg, J. B. C. Pettersson, M. Roeselov, and J. R. Sodeau, Atmos. Chem. Phys. Discuss. **12**, 30409 (2012).
[18]D. D. Davis, J. Seelig, G. Huey, J. Crawford, G. Chen, Y. Wang, M. Buhr, D. Helmig, W. Neff, D. Blake, R. Arimoto, and F. Eisele, Atmos. Environ. **42**, 2831 (2008).
[19]J. L. France, M. D. King, M. M. Frey, J. Erbland, G. Picard, S. Preunkert, A. MacArthur, and J. Savarino, Atmos. Chem. Phys. **11**, 9787 (2011).
[20]J. L. Thomas, J. Stutz, B. Lefer, L. G. Huey, K. Toyota, J. E. Dibb, and R. von Glasow, Atmos. Chem. Phys. **11**, 4899 (2011).
[21]F. Domine and P. B. Shepson, Science **297**, 1506 (2002).
[22]F. Domine, M. Albert, T. Huthwelker, H. W. Jacobi, A. A. Kokhanovsky, M. Lehning, G. Picard, and W. R. Simpson, Atmos. Chem. Phys. **8**, 171 (2008).
[23]R. Ruzicka, L. Barkov, and P. Klán, J. Phys. Chem. B **109**, 9346 (2005).
[24]R. Kurková, D. Ray, D. Nachtigallová, and P. Klan, Environ. Sci. Technol. **45**, 3430 (2011).
[25]V. F. McNeill, A. M. Grannas, J. P. D. Abbatt, M. Ammann, P. Ariya, T. Bartels-Rausch, F. Domine, D. J. Donaldson, M. I. Guzman, D. Heger, T. F. Kahan, P. Klán, S. Masclin, C. Toubin, and D. Voisin, Atmos. Chem. Phys. **12**, 9653 (2012).
[26]P. Nissenson, D. Dabdub, R. Das, V. Maurino, C. Minero, and D. Vione, Atmos. Environ. **44**, 4859 (2010).
[27]Y. Dubowski, A. J. Colussi, and M. R. Hoffmann, J. Phys. Chem. A **105**, 4928 (2001).
[28]H. Beine and C. Anastasio, J. Geophys. Res., [Atmos.] **116**, D14302, doi:10.1029/2010JD015531 (2011).
[29]A. M. Baergen and D. J. Donaldson, Environ. Sci. Technol. **47**, 815 (2013).
[30]T. Blunier, G. L. Floch, H. W. Jacobi, and E. Quansah, Geophys. Res. Lett. **32**, L13501, doi:10.1029/2005GL023011 (2005).
[31]J. Mack and J. R. Bolton, J. Photochem. Photobiol. A **128**, 1 (1999).
[32]E. S. N. Cotter, A. E. Jones, E. W. Wolff, and S. J. B. Bauguitte, J. Geophys. Res., [Atmos.] **108**, 4147, doi:10.1029/2002JD002602 (2003).
[33]H.-W. Jacobi and B. Hilker, J. Photochem. Photobiol. A **185**, 371 (2007).
[34]C. Boxe and A. Saiz-Lopez, Polar Sci. **3**, 73 (2009).
[35]J. Bock and H.-W. Jacobi, J. Phys. Chem. A **114**, 1790 (2010).
[36]J. Lee-Taylor and S. Madronich, J. Geophys. Res. **107**, 4796, doi:10.1029/2002JD002084 (2002).
[37]J. Erbland, W. C. Vicars, J. Savarino, S. Morin, M. M. Frey, D. Frosini, E. Vince, and J. M. F. Martins, Atmos. Chem. Phys. **13**, 6403 (2013).
[38]W. R. Simpson, M. D. King, H. J. Beine, R. E. Honrath, and X. Zhou, Atmos. Environ. **36**, 2663 (2002).
[39]H.-W. Jacobi, T. Annor, and E. Quansah, J. Photochem. Photobiol. A **179**, 330 (2006).
[40]J. D. Burley and H. S. Johnston, Geophys. Res. Lett. **19**, 1359, doi:10.1029/92GL01115 (1992).
[41]T. A. Berhanu, C. Meusinger, J. Erbland, J. Savarino, and M. S. Johnson, J. Chem. Phys. **140**, 244306 (2014).
[42]J. C. Gallet, F. Domine, C. S. Zender, and G. Picard, Cryosphere **3**, 167 (2009).
[43]F. Domine, R. Salvatori, L. Legagneux, R. Salzano, M. Fily, and R. Casacchia, Cold Reg. Sci. Technol. **46**, 60 (2006).
[44]G. J. Phillips and W. R. Simpson, J. Geophys. Res. **110**, D08306, doi:10.1029/2004JD005552 (2005).
[45]M. D. King and W. R. Simpson, J. Geophys. Res. **106**, 12499, doi:10.1029/2001JD900006 (2001).
[46]E. Thibert and F. Domine, J. Phys. Chem. B **102**, 4432 (1998).
[47]L. G. Huey, D. J. Tanner, D. L. Slusher, J. E. Dibb, R. Arimoto, G. Chen, D. Davis, M. P. Buhr, J. B. Nowak, R. L. Mauldin III, F. L. Eisele, and E. Kosciuch, Atmos. Environ. **38**, 5411 (2004).
[48]H. J. Beine, A. Amoroso, F. Domine, M. D. King, M. Nardino, A. Ianniello, and J. L. France, Atmos. Chem. Phys. **6**, 2569 (2006).
[49]S. Goldstein and J. Rabani, J. Am. Chem. Soc. **129**, 10597 (2007).
[50]J. France and M. King, J. Glaciol. **58**, 417 (2012).
[51]D. Madsen, J. Larsen, S. K. Jensen, S. R. Keiding, and J. Thøgersen, J. Am. Chem. Soc. **125**, 15571 (2003).
[52]P. Warneck and C. Wurzinger, J. Phys. Chem. **92**, 6278 (1988).